Behavior- and circuit-specific cortico-striatal decoupling during the early development of Parkinson's disease-like syndrome

Xu-Ran Yao[1,2], Yang Liu[1,2], Wei-Tong Zheng[1,2], Kai-Wen He[1,2,3*]

[1]*Interdisciplinary Research Center on Biology and Chemistry, Shanghai Institute of Organic Chemistry, Chinese Academy of Sciences, 100 Haike Rd, Shanghai 201203, China*

[2]*University of Chinese Academy of Sciences, Beijing 100049, China*

[3] *Shanghai Key Laboratory of Aging Studies, Shanghai 201210, China*

[*] Correspondence: kwhe@sioc.ac.cn

ABSTRACT

Despite that cortico-striatal decoupling has been widely reported in individuals diagnosed with Parkinson's Disease (PD), its onset, circuit specificity and underlying mechanism remain largely unclear. To investigate these questions, dual fiber photometry is established for the first time to evaluate cortico-striatal coupling during varied motor behaviors, whose cell-type resolution was provided by the usage of Cre transgenic mouse lines. Contralateral turning, digging and licking show distinct coupling patterns, among which digging induces the strongest coupling. Striatal D1R-expressed medium spiny neurons (dMSNs) and D2R-expressed MSNs (iMSNs) similarly contribute to the cortical-striatal coupling during turning and licking but not digging, with much tighter coupling between the dMSNs and the M1 cortex. In PD-like mouse model induced via intra-striatal injection of synthetic mouse wildtype α-synuclein preformed fibril (PFF), digging-associated cortical-striatal decoupling emerges as early as 1-month post induction (Mpi), which becomes significant since 2 Mpi and correlates with later-onset behavioral deficit. Notably, impaired dMSNs but not iMSNs mediate this decoupling, which can be rescued by activation of D1 but not D2 receptor. Mechanistically, we found an inverted U-shape decline in striatal dopamine level along the disease development in PFF-injected mice. Supplement with L-DOPA alleviates the decoupling and motor deficit, suggesting that early dopamine deficiency directly contributes to the cortical-striatal decoupling and the associated motor deficit. These findings provide new insights into the temporal profile and mechanisms underlying the PD-associated cortico-striatal decoupling, which has been implicated as functional biomarker for early diagnosis of PD.

Keywords: Parkinson’s disease; α-synuclein; fiber photometry; cortico-striatal coupling; striatal circuit specificity, dopamine.

INTRODUCTION

Parkinson's Disease (PD) is one of the most prevalent neurodegenerative disorders that primarily affects patients' motor function(1, 2). Various brain regions within the basal ganglia loop collaborate to regulate motor behavior(3, 4), with the functional coupling between the primary motor cortex (M1) and the striatum (STR) playing a crucial role in motor planning, execution, and learning(5-7). Functional magnetic resonance imaging (fMRI) revealed the reduced cortico-striatal connectivity, or cortico-striatal decoupling in PD patients(8-10). Furthermore, this PD-associated decoupling is correlated with both disease duration and behavioral impairment of patients(11, 12). Cortico-striatal decoupling is also associated with motor deficits in other disorders such as dystonia(13) and Huntington's disease(14). Together, these findings underscore the importance of understanding the mechanism of cortico-striatal coupling and characterizing the cortico-striatal decoupling associated with diseases.

D1 receptor- and D2 receptor-expressed medium spiny neurons (MSN) are the two main types of neurons in the striatum(15, 16). Both of them receive glutamatergic inputs from the cortex and are considered to play distinct yet debated roles in motor control via activation of the direct and indirect pathway, respectively(17-20). How these neurons contribute to the cortico-striatal coupling during motor behavior requires further investigation. In dopamine-depleted PD rodent models, impaired activities of D1R-expressed MSN (dMSN) and/or D2R-expressed MSN (iMSN) have been reported(21). While some studies found similar changes in both dMSN and iMSN firing(22) or increased similarity between their discharge frequency(23) after dopamine deletion, many others suggest the imbalanced activity between them might be the main cause of motor deficit(24-27). Whether and how dMSN and iMSN contribute to the cortico-striatal decoupling associated with parkinsonian remains to be answered.

81 The intrastriatal injection of α-Syn preformed fibril (PFF) effectively induces aggregation of α-Syn and
82 dopaminergic (DA) neuron cell loss in the substantia nigra (SN), two pathological hallmarks of PD(28)
83 along with motor dysfunction that gradually advances(29-31). This PD-like mouse model allows the
84 monitoring of potential alterations in cortico-striatal coupling preceding the onset of motor deficits.

85 In the present study, we first established a dual fiber photometry system to examine the cortico-striatal
86 coupling with behavioral and pathway specificity. Using the PFF-induced PD-like mouse model, we then
87 analyzed the characteristic as well as the underlying cellular and circuitry mechanism of cortico-striatal
88 decoupling during disease progression. Our findings validate a new method to study functional coupling
89 with cell type and circuit resolution, and for the first time unveil the temporal profile of M1 cortex-dorsal
90 striatum decoupling with the PFF-induced PD-like mouse model, uncover the distinct contributions of
91 dMSN and iMSN.

92

93 **RESULTS**

94 **Dual fiber photometry measures coupling of cortical and striatal activity during different motor**
95 **behaviors**

96 Several techniques, including electroencephalography (EEG), local field potential (LFP), and fMRI,
97 have been utilized to assess the coupling between neural activities in various brain subregions(32-34).
98 However, these approaches are limited in their capacity to elucidate the circuitry mechanisms
99 underlying such coupling. Considering that striatal neurons predominantly comprise dMSNs and iMSNs,
100 there is a pressing need for a novel method to explore the cell type-specific cortico-striatal coupling
101 during motor behavior in both healthy and diseased brains.

102 To address this challenge, we employed fiber photometry, which allows for the concurrent monitoring of
103 activity across different cell types in multiple brain regions in behaving mice(35). Two calcium indicators,
104 jRGECO1a and GCaMp7s, were respectively expressed in neurons in the deeper layers of the primary
105 motor cortex (M1) and dorsal striatum (STR) of the same hemisphere, followed by the implantation of
106 two optical fibers (Fig 1A-B; see Methods). Utilizing this dual fiber photometry approach, we successfully
107 monitored neuronal activities of M1 and the dorsal striatum without discernible crosstalk of fluorescence
108 signals (Fig 1B, Supplementary Figure 1A). Three naturalistic mouse motor behaviors, namely contra-
109 lateral turning, licking, and digging, were chosen to investigate cortico-striatal coupling (Fig 1C, 1G, 1K).
110 The coupling index is determined by calculating the Pearson's correlation coefficient between the
111 activities of the two channels within a time window around behavior initiation. Additionally, the phase
112 lag is estimated to assess the temporal alignment of the two responses (see Methods). Contralateral
113 turning has been demonstrated to elicit a striatal response(36). Fibers in the striatum consistently
114 detected robust neuronal activity in response to turning initiation (Fig 1D, right), validating the temporal
115 resolution of fiber photometry for monitoring fast motor behavior-evoked neuronal activity. Interestingly,
116 M1 neuronal activity was suppressed mildly during contralateral turning (Fig 1D, left), resulting in a
117 negative coupling between M1 and the striatum (Fig 1E; see Methods). In contrast, both M1 and the
118 striatum were activated during licking, with the striatal response exhibiting slightly earlier onset and
119 being more phasic compared to M1's response (Fig 1H-I). The distinct dynamics of these responses
120 consequently resulted in a coupling index close to 0 for licking behavior (Fig 1J). During digging, where
121 mice retrieved food pellets buried underneath the bedding (see Methods), both M1 and the dorsal
122 striatum exhibited robust activation upon initiation (Fig 1L). The digging-induced responses from both
123 channels were temporally aligned (Supplementary Figure 1C) and exhibited similar kinetics (Fig 1M),

124 reflected by a coupling index close to 1 (Fig 1N).

125 Thus, we have developed a dual fiber photometry approach to investigate the activity coupling between
126 M1 and the striatum. Our findings reveal distinct coupling patterns, implying that complex rules govern
127 cortico-striatal communication during various motor behaviors.

128 **dMSNs and iMSNs distinctively contribute to the cortico-striatal coupling in different motor**
129 **behaviors**

130 To investigate the cell type-specific cortico-striatal coupling, GCaMp7s was selectively expressed in
131 either striatal dMSNs or iMSNs by using D1R-cre or D2R-cre mice (Fig 2A-B, see Methods). The dual
132 fiber photometry system recorded clear calcium activities from M1 neurons and striatal dMSNs or iMSNs
133 concurrently (Supplementary Figure 2A-B). Both striatal dMSNs and iMSNs were similarly activated
134 upon contralateral turning and licking (Fig 2C, E), and their coupling with M1 activity remained
135 consistent across cell types (Fig 2D, F). These findings suggest that both cell types in the striatum
136 participate similarly in these two behaviors, consistent with previous studies (36-38). During digging
137 behavior, striatal dMSNs exhibited digging-evoked activity closely resembling that of total striatal
138 neurons and tightly coupled with M1 activity (Fig 2G-H). Notably, although iMSNs exhibited regular
139 activity during free moving (Supplementary Figure 2B), contralateral turning and licking, they displayed
140 a much weaker response during digging (Fig 2G) and significantly reduced coupling with M1 activity
141 compared to that of dMSN-M1 (Fig 2H). These findings further underscore the importance of
142 investigating cell type-specific M1-striatal coupling in motor behavior.

143 **Intrastriatal injection of α-syn PFF induces PD-like pathology in wildtype mice**

144 Cortico-striatal decoupling has been widely reported in patients with mild to severe Parkinson's disease

145 (PD), correlating positively with motor impairment(11, 39, 40). To investigate the onset and mechanism
146 underlying this PD-associated cortico-striatal decoupling, we adapted an inducible PD-like mouse
147 model established previously(41) by bilaterally inoculating α-synuclein (α-Syn) preformed fibrils (PFF)
148 into dorsal striatum of wildtype mice (Fig 3A). Behavioral and pathological phenotypes were examined
149 at both one- and three-month post PFF inoculation (Fig 3B). One-month post-injection (1Mpi), PFF led
150 to a slight reduction in rotarod learning ability (Fig $3C_1$) without affecting the rotarod test performance
151 (Fig $3C_2$) or the general locomotor activity (Fig $3C_3$). By 3-month post-injection, mice receiving PFF
152 displayed notable motor deficits (Fig $3D_1$, D_2), indicating a progressive PD-like motor impairment.
153 Concurrently, we assessed two pathological hallmarks of PD, α-Syn aggregates, and dopaminergic
154 neuron loss, via immunohistochemistry. PFF inoculation in striatum induced significant increase in the
155 phosphorylated α-Syn immunoreactivity (p-α-Syn), a common marker for synucleiopathy, both 1- and
156 3-month post injection in both the striatum (Fig 3E-F, L-M) and the substantia nigra (SN) (Fig 3H-I, O-
157 P). The rapid formation and spreading of synucleiopathy coincided with a progressive reduction in
158 striatal dopamine transporter (DAT) signal intensity in the striatum (Fig 3G, N) and a decreased in
159 dopaminergic neuronal cell count in SN (Fig 3J, Q). These findings confirm that PFF can initiate the
160 formation of α-Syn aggregates, which can further spread to the SN and trigger the pathology of
161 dopaminergic neurons in a time-dependent manner.

162 **Behavior-specific cortico-striatal decoupling emerges early in the PFF-injected mice**

163 Utilizing the PFF-induced PD-like mouse model, we aimed to investigate the onset timing and
164 mechanisms underlying cortico-striatal decoupling during disease progression by using the dual fiber
165 photometry method. PFF inoculation had no discernible effect on the fiber-based calcium imaging
166 (Supplementary Figure 3A-C). Given its robustness and circuitry dependency, we compared digging-

evoked M1-dorsal striatum coupling between PFF and PBS-injected mice. At one month post-injection, cortico-striatal coupling largely persisted (Fig 4B-C), albeit with a moderate increase in trial-by-trial phase lags among PFF mice compared to PBS counterparts (Fig 4B, C_3), indicating the emergence of early temporal decoupling. By the second month post-injection, PFF mice exhibited a further increase in phase lag relative to PBS controls (Fig 3D, E_2, E_3), accompanied by a declining trend in the cortico-striatal coupling index (Fig $4E_1$) while cortical and striatal response amplitudes remained unchanged (Supplementary Figure 3E). Following three to four months of PFF inoculation, decoupling in PFF mice worsened, contrasting with sustained tight coupling observed in PBS mice between M1 and the striatum during digging (Fig 4F, G_1). This decoupling in PFF mice were attributed to both elevated phase lag (Fig $4G_2$, G_3) and a significant reduction in striatal response amplitude (Fig 4H). Temporal profiles of the coupling index (Fig 4I, left), phase lag (Fig 4I, right), and response amplitude (Supplementary Figure 3F-G) collectively suggest an initial impairment in temporal precision of cortico-striatal communication in this PD-like mouse model, with cortico-striatal decoupling exacerbating as pathology progresses. We subsequently investigated whether the cortico-striatal decoupling in digging affect the digging behavior. Digging duration and frequency were quantified and compared between groups (See Methods). It was found that until three months post-injection PFF mice exhibited a shortened digging duration (Fig 5A) and increased frequency (Fig 5B) relative to the PBS controls. Furthermore, the phase lag and coupling index, but not the striatal response amplitude (Supplementary Figure 4C-D), strongly correlated positively (Fig. 5C) and negatively (Fig. 5E) with digging frequency. Conversely, they exhibited opposite correlations with digging duration (Fig 5D, F). These findings suggest that the functional decoupling between M1 and dorsal striatum emerges early, predicting the later-onset behavioral deficit.

Of note, although the cortico-striatal coupling during digging was compromised in PFF mice, it remained

189 unaltered during licking even after 4 months of PFF injection (Fig 4K-M, Supplementary Figure 3H), at
190 which point PFF mice displayed normal licking behavior (Supplementary Figure 4E-H). This result
191 suggests that the PD-associated decoupling and motor deficit at early stages is behavior-specific.

192 **Defects in dMSN neuronal activity mediates the digging-associated cortico-striatal decoupling**
193 **in PFF-injected mice**

194 A functional imbalance between the dMSNs and iMSNs has been proposed to underlie the bradykinesia
195 in PD patients(16). Therefore, we explored whether there is a cell-type effect in the observed early-
196 onset cortico-striatal decoupling in the PFF-induced PD-like mice. To investigate this, we employed a
197 methodology akin to that depicted in Figure 2A (Fig 6A). Additionally, D2R-Cre mice were also utilized
198 to examine the M1-dMSN coupling by expressing CreOFF-GCaMP in the striatum (See Method), which
199 could effectively label dMSNs (Supplementary Figure 5A) and generate reliable dMSNs responses
200 during various behaviors (Supplementary Figure 2C-F, Supplementary Figure 5B). We then tracked
201 cortico-striatal coupling in a pathway-specific manner beginning at 2 months post-injection, when
202 decoupling becomes apparent in PFF mice. The findings revealed that digging-related cortical and
203 striatal dMSN responses were markedly decoupled in PFF mice as early as 2 months post-injection
204 (Fig 6B), as evidenced by a significantly decreased coupling index (Fig 6C_1) and an increased phase
205 lag (Fig 6C_2). This M1-dMSN decoupling exacerbated further at 3~4 months post-PFF injection,
206 coinciding with a notably diminished striatal dMSN response compared to PBS mice (Fig 6D-E). In
207 contrast to the M1-dMSN decoupling, coupling between M1 and striatal iMSN during digging remained
208 largely unaffected in the PFF mice throughout the experimental time course (Fig 6F-J), indicating a cell
209 type-selective impairment in dMSNs contributing to the cortico-striatal decoupling in this PD-like mouse
210 model. Moreover, PFF inoculation had no discernible effect on the licking-evoked coupling between M1

211 and dMSN or iMSN (Supplementary Figure 5G-H), suggesting that cell-type-specific cortico-striatal
212 decoupling in PD is also behavior-specific.

213 **Altered locomotion-associated striatal dopamine level in the PFF-injected mice**

214 Insufficient striatal dopamine released from SN dopaminergic terminals is the primary cause of the
215 disturbed basal ganglia circuit that mediates the motor deficits in PD(16). Recent studies have indicated
216 a correlation between dopamine depletion and abnormal functional connectivity in both rodent models
217 and PD patients(42-45). Consequently, we hypothesized that abnormal dopamine level might underlie
218 the early-onset, cell-type-specific cortico-striatal decoupling observed in PFF-induced PD mice. To
219 monitor extracellular dopamine level at various time points, we expressed the dopamine sensor DA4.4
220 in striatal neurons (Fig 7A-B). In PBS mice, the fluorescence signal remained stable throughout the 3-
221 month recording period (Supplementary Figure 6A). The extracellular dopamine level was first
222 examined when PFF and PBS mice freely explored new cages (Fig 7C). PFF mice exhibited normal
223 general activity (Supplementary Figure 6B) and unaltered dopamine signals (Fig 7D-E), measured as
224 the summation of the fluorescent intensity during the exploration (see Methods). Since exploration of
225 new environments primarily triggers novelty-seeking behavior driven by dopamine release from the
226 ventral tegmental area (VTA)(46, 47), these findings suggest minimal impact of PFF inoculation on VTA-
227 mediated dopamine release up to 3 months post-injection. Dopaminergic neurons in the substantia
228 nigra compacta (SNc) are pivotal for voluntary movement(40, 48). To assess whether dopamine release
229 by SNc dopaminergic neurons is affected, mice were trained to run at a constant speed on a treadmill
230 (Fig 7F). Both PBS and PFF mice maintained their performance up to 3-month post-injection
231 (Supplementary Figure 6C). Interestingly, dopamine signal during constant speed running exhibited a
232 inverted U-shaped pattern of changes in PFF mice compared to PBS mice, with significant reductions

233 at 3-4 weeks and 10-14 weeks post-PFF injection, but a transient recovery at 6-7 weeks (Fig 7G-H).
234 These findings suggest impaired SNc-mediated dopamine release in PFF mice.

235 **Activation of D1R but not D2R rescues the cortico-striatal decoupling and behavioral defects of**
236 **the PFF-injected mice**

237 To investigate whether the impaired dopamine release is responsible for the dMSN-mediated cortico-
238 striatal decoupling and related behavioral deficit, PFF mice at 4-month post-injection received
239 intraperitoneal (i.p.) administration of L-dopa, SKF-81297 (SKF, a D1R receptor agonist), quinpirole
240 (Quin, a D2R receptor agonist), or saline (SAL) (Fig 8A). Consistent with our previous findings, both L-
241 dopa and SKF, but not Quin, rescued the digging-associated decoupling phenotypes, reflected by
242 decreasing phase lag (Fig 8C) and a trend of increasing coupling index in PFF mice (Fig 8D). Besides,
243 SKF but not Quin enhanced the striatal response amplitude in them (Fig 8E). These results further
244 support the notion that at this stage of PD development, deficient striatal dopamine leads to cortico-
245 striatal decoupling via impairing dMSN neuronal activation during digging.

246 Subsequently, the behavioral effects of these drugs were tested. Both L-dopa and SKF improved the
247 digging performance of the PFF mice (Fig 8F-G) without changing their general locomotion
248 (Supplementary Figure 7C). Moreover, SKF significantly increased the success rate, further supporting
249 that targeting dMSNs alone is more beneficial for the digging behavior (FigureS7D). In contrast, Quin
250 did not rescue the digging performance (Fig 8F, Supplementary Figure 7D), consistent with the absence
251 of digging-associated M1-iMSN decoupling in PFF mice.

252

253 **DISCUSSION**

254 Many clinical studies have revealed abnormal cortico-striatal functional coupling in patients diagnosed

255 with Parkinson's disease(8-11), among which the decoupling between M1 and striatum has been found
256 to tightly correlate with parkinsonian(49-51) even in the early stages of the disease(51). Therefore,
257 abnormal brain connectivity has been proposed as a functional biomarker for early diagnosis of
258 neurodegenerative diseases including PD(52, 53) and Alzheimer's disease(54, 55). The phenotypic
259 characterization and the underlying mechanistic investigation of such decoupling in PD animal model
260 may provide insight to facilitate not only the early diagnosis but also intervention.

261 Despite the development of various methods to detect inter-region brain coupling, such as LFP, EEG,
262 and fMRI(56), none of these techniques offer cell type-specific precision. Our current study establishes
263 a dual fiber photometry imaging method to investigate M1-striatal coupling with circuitry resolution by
264 using cell type-specific cre mouse lines. Although photometry imaging has lower temporal resolution
265 compared to LFP and EEG(57, 58), our method demonstrates its capability of differentiating distinct
266 M1-striatal coupling patterns associated with different motor behaviors (Fig 1). Among the three
267 behaviors, spontaneous contralateral turning as a reflexive behavior(59) evokes striatal but no obvious
268 M1 response, resulting in the weakest coupling reflected by the negative coupling index. Both tone-
269 cued licking and food pellet-driven digging evoke strong M1 and striatal activities, which are tightly
270 coupled with each other in particularly during digging. Interestingly, we found that only coupling
271 associated with digging, but not the other two motor behaviors with relatively weak coupling, displays
272 early abnormality in the PD-like mice. These findings suggests that motor tasks requiring effective
273 cortico-striatal co-activation might facilitate the early detection of PD-like pathological decoupling, which
274 is supported by neuroimaging studies showing task-related fMRI such as finger tapping(50, 60, 61)
275 detects abnormal brain activity and/or connectivity in early-stage PD(62).

276 Our current method further allows us to determine the contribution of dMSNs and iMSNs to the cortico-

277 striatal coupling. Consistent with previous studies(37, 63), we found that both types of MSNs were
278 activated during contralateral turning and licking, validating the accuracy of our method. Such co-
279 activation results in comparable contributions of dMSNs and iMSNs to the cortico-striatal coupling
280 during these behaviors. In contrast, our results reveal that M1 couples much more strongly with dMSNs
281 than iMSNs during digging behavior, mainly due to the greater and more timely activation of dMSNs.
282 Our findings are in line with previous studies using methods such as in vivo two-photon imaging (64) or
283 cell type specific optogenetic manipulation(19) that show distinct activation patterns of the dMSNs and
284 iMSNs during motor behaviors such as lever pressing(19, 64). Therefore, by simultaneously monitoring
285 M1 and striatal dMSNs or iMSNs activities, we provide evidences for the first time that the M1-striatal
286 coupling is regulated in a behavior- and circuit-specific manner.

287 Among all three motor behaviors we tested, only cortico-striatal coupling associated with digging is
288 impaired even before the behavioral deficit manifested. Digging is also the only behavior evoking
289 unequal activity of dMSNs and iMSNs. which may render it more susceptible to PD pathology. Striatal
290 MSNs form functional units, whose activity is responsible for driving specific behavior and is tightly
291 regulated by the complex lateral inhibitory network(65). Indeed, we found the significantly impaired
292 digging-evoked dMSN but not iMSN activity correlates with the behavioral deficit. It is noteworthy that
293 the phase lag, a parameter describing the relative timing of the M1 and striatal responses, shows the
294 strongest correlation with the digging performance (Fig 5C-F). This suggest that the effective
295 connectivity between the M1 and the striatum also, if not more, potently regulates specific behaviors.

296 Weakening of dMSNs while strengthening of iMSNs is observed in PD rodent models mimicking late
297 stages of PD, which lead to imbalance activity of the direct and indirect pathways and are considered
298 to mediate the motor dysfunction in PD(16, 66). Here we found that the activity of dMSNs but not iMSNs

299 is impaired during digging early in the PFF-induced PD-like mice. A previous study also found a selective
300 disconnection of dMSNs but not iMSN with the M1 in a 6-OHDA-induced partial dopamine lesion mouse
301 model(67). These findings together suggest that dMSNs might be more vulnerable at the early stages
302 of PD development. Interestingly, recent research has demonstrated that gene therapy selectively
303 activating striatal dMSNs can effectively reverse PD-like symptoms in both rodent and primate models
304 of PD(68). Here we also showed that administration of D1R agonist but not D2R agonist, rescued both
305 the digging-associated decoupling and behavioral deficits. Therefore, dMSNs might be better targets
306 for early PD intervention.

307 The lack of dopamine (DA) from SN dopaminergic terminals in the striatum can cause dysfunction in
308 the basal ganglia circuit and consequently lead to motor defects in PD patients(16, 69-71). Research
309 has revealed abnormal coordination between cortical and striatal ensembles in acutely dopamine-
310 depleted mice(72). Moreover, a clinical study reported an increase in M1-putamen connectivity after L-
311 DOPA intake in some PD patients(73). These findings collectively link the cortico-striatal coupling with
312 DA level in the PD state. In fibril-induced PD-like mice, a reduction in dopaminergic neurons in SNpc
313 begins as early as 4 weeks post inoculation, which is consistent with a significant reduction in the striatal
314 DA level during constant speed running. Interestingly, DA release transiently recovers 6-7 weeks post
315 inoculation, potentially due to a compensatory increase in spiking of the remaining dopaminergic
316 neurons in the SNpc(74). Therefore, the impaired DA level during motor behavior may mediate the
317 decoupling and behavioral deficit observed in the PD-like mice. Indeed, supplement of L-dopa almost
318 fully rescues these defects. Accumulating evidence suggests that abnormal axonal dopamine release
319 could occur before dopaminergic cell lost(71, 75), further supporting the notion that dopamine-
320 dependent, motor task-specific cortical-striatal decoupling might serve as an functional biomarker for

321 early PD.

322 Another mechanism regulating the cortico-striatal coupling might involve striatal fast-spiking
323 interneurons (FSIs), who is well known to dictate the temporal precision of neural information
324 processing(76-78). Within the striatal functional units that drive specific motor behavior, potent lateral
325 inhibitions are provided by the soma-targeting FSIs in addition to the MSN collaterals(65). In addition,
326 these FSIs are found to be activated faster with lower thresholds compared to MSNs(79, 80), making
327 them ideal for regulating the timing and dynamic of the striatal response. Moreover, FSI activity is
328 sensitive to DA(81) and its alteration has been shown to exacerbate striatal imbalance(24). It remains
329 to be determined whether the impaired DA level in the early stage of PD affects cortico-striatal coupling
330 by altering FSI activity.

331

332 **CONCLUSION**

333 Our study establishes a methodology utilizing fiber photometry to detect motor task-driven inter-regional
334 brain coupling with cell-type resolution. By employing this approach, we reveal the behavior-specific
335 M1-striatum decoupling preceding the behavioral deficit in the α-Syn PFF-induced PD-like mice,
336 supporting the use of motor task-specific cortico-striatal decoupling as a functional biomarker of early
337 PD. Additionally, we found that the decoupling associated with digging is selectively mediated by
338 impaired dMSNs in a dopamine-dependent manner, unveiling for the first time the circuitry mechanism
339 mediated task-specific decoupling in the PD state.

340

341 **Acknowledgement**

We thank Dr. Cong Liu and his students for their help in preparing the PFF. We also thank the staff members of the animal facility at the National Facility for Protein Science in Shanghai (NFPS), Shanghai Advanced Research Institute, Chinese Academy of Sciences, China for excellent support. This work is supported by NSFC (Grant No. 32271004, 32070963), and Shanghai Municipal Science and Technology Major Project (Grant No. 2019SHZDZX02) to K.-W.H.

Author contributions

Conceptualization, K.-W.H.; Primary Investigation, X.-R.Y.; Assistant Investigation, Y.L., W.-T.Z.; Data Analysis, X.-R.Y., Y.L.; Writing, X.-R.Y., Y.L. and K.-W.H.; Funding Acquisition, K.-W.H; Supervision, K.-W.H.

List of abbreviations

PD	Parkinson's disease
M1	Primary motor cortex
Str	Striatum
SN	Substantia nigra
DA	Dopamine
DAT	Dopamine transporter
D1R	Type 1 dopamine receptor
D2R	Type 2 dopamine receptor
MSN	Medium spiny neuron
dMSN	direct pathway MSN

iMSN	indirect pathway MSN
α-Syn	α-Synuclein
PFF	Preformed fibril
Mpi	Month(s) post injection

METHODS

Animals

All procedures were approved by the Institutional Animal Care and Use Committees at the Interdisciplinary Research Center on Biology and Chemistry (IRCBC), Chinese Academy of Science. C57BL/6J mice were purchased from Shanghai Lingchang Biotechnology Co., Ltd.. The transgenic mice (D1R-Cre: MMRRC_034258-UCD; D2R-Cre: MMRRC_034258-UCD) were bred in-house. Mice were group housed with a 12 h:12 h light:dark cycle and ad libitum access to food and water until experiments. Male mice of 2-8 months of age were used with exception stated specifically. All experiments were carried out at ZT (Zeitgeber time) 15~19.

Preparation and characterization of mouse wildtype α-Syn PFF

The procedures followed the same protocol as described previously(31). In brief, pET22 vector plasmid containing α-syn gene was transfected into BL21 (DE3) cells. α-syn expression was induced by IPTG (isopropyl-1-thio-D-galactopyranoside). Cells were then harvested and sonicated followed by boiling, streptomycin (20 mg/mL) treatment, pH adjustment, and dialysis overnight in turn. The α-syn monomer was then incubated in solution containing 100 μM in 50 mM Tris, pH 7.5, 150 mM KCl, and 0.05% NaN3 buffer at 37 °C with constant agitation (900 rpm) in ThermoMixer (Eppendorf) for one week to form fibril

386 structure. The fibril was quantified by subtracting the residual soluble α-syn from the total amount of α-
387 syn monomer and the fibril pellet was suspended with PBS to 2 μg/μL. The obtained fibril was sonicated
388 (20% power 15 times (1 s on, 1 s off) on ice, JY92-IIN sonicator) and the structure was confirmed by
389 TEM (FEI Company, USA).

390 **Stereotaxic injection**

391 Craniotomy was performed as described previously(31, 76). Briefly, mice were anesthetized with
392 isoflurane vapor (1~2% in air) and head-fixed in a stereotaxic frame (RWD Life Science, China) with
393 heating pad (~37 ºC) underneath to maintain body temperature. The scalp was removed, and
394 virus/fibril/PBS was delivered at a rate of 80 nl/min to either M1 (bregma/midline/depth: 1.77/1.5/-0.67
395 mm) or dorsal lateral striatum (dlSTR. For GCaMP7s: -0.11/2.5/2.3 mm; for PFF/PBS, DA sensor,
396 0.2/2.0/2.6 mm) by using a glass pipette connected to a micro syringe pump (Stoelting, USA). For
397 photometry calcium imaging, 150 nl of AAV-hSyn-NES-jGRECO1a was injected into M1 layer V; 350 nl
398 of AAV-hSyn-GCaMP7s (or 400nL AAV-hSyn-DIO-GCaMP7s for Cre mice) was injected into dlSTR. To
399 measure the striatal extra-cellular dopamine level, 400nl of AAV-hSyn-GRabeen-DA4.4 was injected
400 into dlSTR. All viruses were diluted to a titer of 10^{12} vg./ml. For establishing the α-Syn PFF model, PFF
401 or PBS (0.1 μl/g body weight, 2.5 μl at most) was injected at a speed of 0.5 μl/min for the first 0.2 μL
402 and 0.2 μL/min for the rest.

403 **Fiber photometry surgery and imaging**

404 Optical fibers (NA: 0.37; diameter: 200μm; Inper, China) were implanted using the same M1 and dlSTR
405 coordinates except 0.05 mm less in depth right after the virus injection. Fiber was secured to the skull
406 using dental cement (C&M Super Bond, Japan). Mice were then housed individually and allowed to
407 recover for at least 2 weeks before imaging.

Photometry recording during behavioral paradigms was conducted during the dark cycle utilizing a commercial multichannel fiber photometry system (Inper, China). Excitation light at wavelengths of 470 nm, 561 nm, and 410 nm was used to excite GCaMP7s/DA-4.4, RGECO1a, and Ca^{2+}-independent internal channel control, respectively. Fluorescence signal was collected at 40 Hz using InperStudio (MultiColorEVAL15) software, which automatically synchronized the calcium signal with video footage from a camera positioned above the arena. Throughout the imaging, the patch cord attached to the optical fiber was suspended by a helium-filled balloon to minimize its weight impact on the mouse behavior. All behavioral trials lasted for less than 30 min.

Immunofluorescence (IF) staining

IF was performed as previously describe(31). Briefly, mice were anesthetized with isoflurane vapor and perfused with PBS followed by about 40 ml of 4% paraformaldehyde (PFA). Subsequently, whole brain was removed and fixed overnight in PFA at 4°C. The fixed brains were then saturated in PBS containing 20% sucrose for overnight to ensure the mice brains sinking bottom, and 30% sucrose for 2 d. Afterward, the brains were embedded in tissue freezing medium (OCT, Leica) and rapidly frozen and stored at -80°C. Next, 20 μm coronal slices were sectioned using the cryostat (Leica, CM3050s-1-1-1). These sections were incubated in blocking solution (PBS containing 5% normal goat serum (Sigma) and 0.1% Triton X-100) for 2 hours at room temperature, followed by overnight incubation at 4°C with the primary antibody diluted in the blocking solution. After incubation, the primary antibody solution was washed out three times with PBST (0.1% Tween-20 in PBS) and once with PBS, followed by incubation with the fluorophore-conjugated secondary antibodies for 2 hours at room temperature. For MSN type-specific labeling, DAPI (diluted at 1:500) was then used to stain the nuclei for 10 minutes at room temperature. Information of all antibodies used were summarized in Supplementary Table 1.

To validate the expression and location of the calcium and dopamine sensor, PFA-fixed brains were

sectioned into 60 μm coronal slices using a vibratome (Leica VT 1000S). Slices with optical fiber track were selected for subsequent fluorescence imaging. Slices were further stained for either D1R or D2R for cell-type specific colocalization.

Confocal Imaging

Fluorescence images were captured using a spinning disk confocal microscope (Andor, UK). Different lasers with wavelengths of 630 nm, 561 nm, 488 nm, and 405 nm were sequentially utilized to excite the Fluor 647, Fluor 568 or RGECO1a, Fluor 488 or GCaMP7s or DA4.4, and DAPI respectively. Imaging was performed using a 20× air (NA = 0.75), or 40× water (NA = 1.25) objective, with consistent settings maintained for each set of experiments. The image resolution is 0.6 μm:0.6 μm/pixel (x:y) for 20× and 0.15 μm:0.15 μm/pixel (x:y) for 40× objective. Z-stack images were acquired for all brain regions and then projected in the z-direction to obtain the maximum intensity for subsequent analysis in ImageJ. Step size (μm) and thickness (μm) of each brain region were as followed: SN: 0.5, 1; Striatum: 1, 5 (for characterization of the PFF-induced pathology); Others: 2, 10. The whole view of STR was analyzed, while the SN region was manually selected based on the mouse brain atlas. The average intensity of phosphorylated α-synuclein (P-α-syn) and dopamine transporter (DAT) was measured using the same background subtraction and contrast transformation applied to each dataset, and then normalized to the control (PBS group). DAT-positive dopamine neurons in the Substantia Nigra pars compacta (SNpc) were automatically selected and counted using the Spot module of Imaris (Oxford Instruments), with settings consistent with previous descriptions(41).

Behavioral task or test

a. Digging test

Mice were food deprived for 24h before behavioral digging test. During the deprivation, two food pallets (25mg, sucrose and milk powder in a 1:1 ratio. Xietong Bio-engineering Co., Ltd., China) were placed in its home cage to introduce novel food. The test environment consisted of a lidless, semitransparent box (FENGSHI group, China), identical in size and texture to the mouse's home cage (l:w:h: 29 cm×18 cm×13 cm), serving as the arena for the digging test. The bottom of the arena was covered with approximately 3cm-thick clean bedding, and twelve food pallets were evenly buried in the bedding. Additionally, a solitary food pallet was strategically positioned at the center of the arena's surface on top of the bedding, easily accessible for the mice upon entering the arena, thereby enticing them to dig for buried pallets. The mice's performance in the arena was recorded using two cameras—one providing a top view and the other a side view—for subsequent post-hoc analysis. After completing the test, the bedding was discarded, and the arena was cleaned with 75% ethanol.

b. Sound-cued licking task

Mice were habituated and trained for three days prior the final experiment.

Day0. Completely water deprivation

Day1. Mice were required to lick water from the water outlet connected to a sensor. Once the mice lick the outlet, a single dose of 5μl water was pumped out from the outlet. Each mouse repeated this process 100 times.

Day2. A sound cue (3000Hz, 200ms) with random interval (10-20 s) was introduced, and mice had to associate it with water. 5μl water was pumped out if mice licked the outlet within 3s after the cue; otherwise, they received nothing. A 5-second interval allowed mice to consume the water before moving to the next random time interval. Each mouse was allowed to complete 80 water trials

Day3. The random time interval from Day 2 was replaced with a 5-second non-licking interval. Mice had to refrain from licking the outlet for 5s to trigger the sound cue. If they licked during this interval, they had to wait another 5s for the sound cue. The time window for mice to respond to the cue and to consume water remained the same as Day 2. Each mouse was allowed sufficient time to complete 120 watered trials.

Day4. Fiber photometry recording was conducted while mice performed the task, following the paradigm of Day3. The timestamp of licks within each watered trial (see Supplementary Figure 4) was recorded by a sensor controlled by customized Arduino code. The initiation of licking was defined as the first lick detected by the sensor after the sound cue.

c. Rotarod

The procedures followed the protocol described in a previous report(31). Briefly, mice underwent three days of training, consisting of two adaptive trials at a low rolling speed of 5 rpm/min, followed by a third trial with accelerating speed ranging from 0 to 40 rpm/min. After a rest day on the fourth day, mice were tested twice on the rotarod on the fifth day. Each testing session lasted for a total of 5 minutes. During the first 1.5 minutes, the speed of the rotarod accelerated from 0 to 40 rpm/min, which was maintained for the remaining time. Mice were tested twice, and the maximum duration they stayed on the rotarod was recorded for final analysis. Between each trial, the rotarod was thoroughly cleaned with 75% alcohol.

d. Open field test

After a period of habituation, mice were introduced into the center of the open field chamber (40 × 40 cm) and given 10 minutes to freely explore its surroundings. After the test, the arena was cleaned with 75% ethanol. Their activities were observed and recorded using a camera positioned on the

498 ceiling, and the data were subsequently analyzed using EthoVision XT 11.5 software (Noldus,
499 Netherlands).

500 **e. Free exploring in a new cage**

501 The procedures and settings for the open field test were replicated with the exception of utilizing a
502 lidless and empty cage resembling to the mouse's home cage (l:w:h: 29 cm×18 cm×13 cm) as the
503 arena.

504 **f. Free moving**

505 The procedures and settings were exactly same with free exploring but the arena covered with clean
506 bedding.

507 **g. Treadmill running**

508 Mouse was placed on the treadmill (Zhenghua Biologic apparatus, China) 10mins before testing for
509 habitation. During the test, the rolling velocity of conveyor was constantly 10m/min and the testing
510 session would last for 10mins. To prevent interaction between mice, each mouse was isolated by
511 baffles while running on the treadmill. After the test, conveyor and baffles were cleaned with 75%
512 ethanol. Both male and female mice were included in this experiment but they were separated by
513 gender during the test. Any mice that failed to keep up with rolling conveyor during the test was
514 excluded from the analysis.

515

516 **Pharmacology**

517 The experimental design followed a previous study that investigated the effects of dopaminergic drugs
518 on striatal MSNs using calcium imaging in parkinsonian mice(26). The drugs (all compounds from
519 Merck), including D1R agonist (SKF81297; 1mg/kg), D2R agonist (quinpirole; 0.5mg/kg), L-DOPA

520 (1mg/kg) together with benserazide (15mg/kg), were dissolved in 0.9% saline and filtered through a
521 PES membrane filter unit (0.22μm, Millex). These solutions were stored at 4℃ and used within a week.
522 The drugs were administered via intraperitoneal (i.p.) injection, with a volume determined according to
523 body weight (0.1 ml/10 g). Both behavioral and photometry experiments commenced 15 minutes after
524 i.p. except quinpirole (60 minutes post i.p.). Information of all chemicals used were summarized in
525 Supplementary Table 1.
526

527 **Quantification and statistics**

528 **Behavioral analysis**

529 Digging behavior. Trials was manually picked from the video by the investigator. The initiation of
530 digging behavior was determined when the bedding beneath the paws of the mice were visibly displaced.
531 The termination of a digging trial was defined as either no bedding displacement for 1 second or the
532 mice engaging in any other behaviors such as rearing, grooming, or eating pallets. The average duration
533 of all digging trials within the first ten minutes after the mice acquired the pallet on the top of the bedding
534 was considered as the digging duration. Digging frequency was defined as the number of digging per
535 minute during this period. The success rate was calculated as the percentage of trials in which the mice
536 successfully obtained the pallet out of the total number of trials.
537 Licking behavior. It was recorded using a touch sensor controlled by an Arduino chip, with each lick
538 automatically captured and timestamped. The data were then written into a text file. Customized R code
539 was used to analyze the data from the text file and calculate various metrics to characterize licking
540 behavior. A series of successive licks with intervals less than 1 s was considered as a bout. The duration
541 of a bout was defined as the bout length.

Qualitative analysis of photometry signal

a. *Photometry signal processing*

The photometry data collected was pre-processed for bleaching and motion correction using InperDataProcess v0.7.2 software. The onset of digging and contra-turning behavioral events was manually marked based on the synchronized videos. For digging behavior, only trials having ≥ 10 s of dig-less baseline and ≥ 3 s of digging were selected for final analysis. For turning behavior, only trials with ≥ 4 s intertrial interval and ≥ 90 degree turning were chosen for final analysis.

All fiber signal was presented as dF/ F_0 using the equations:

$$\mathrm{dF/F_0} = \frac{F - F_0}{F_0}$$

F represents the fluorescence value of each timepoint. F_0 is the average of F of baseline.

For digging and licking behavior, the time window was -5 to 5 seconds (relative to behavior initiation), during which the -4 to -2 s was used to calculate the F_0. For contra-turning, the time window was -1 to 1 second, and the baseline was -1 to 0 s.

The data were further transformed into z-score using the formula to better compare the dynamic of M1 and striatal responses:

$$\mathrm{Z} = \frac{\mathrm{F} - \overline{\mathrm{F}}}{\sigma}$$

Where $\overline{\mathrm{F}}$ is the population mean, and σ is the population standard deviation.

b. *Coupling index & Phase lag.*

The coupling index represented the Pearson's correlation coefficient of time-aligned averaged M1 and STR signals. It was calculated using the R cor function. Additionally, the ccf function in R was utilized

to determine the lag at which the maximum cross-correlation between the signals occurred. The lag.max parameter was set to be twice the sampling rate.

c. *Plateau & peak amplitude*.

The plateau amplitude was defined as the mean of the normalized (dF/F_0) signal within the plateau stage (1~2 s, relative to initiation) for digging behavior. For licking behavior, the peak amplitude was that within 0~0.5s.

d. *Sum dFF activity*.

The data of each mouse collected during 10 minutes of treadmill running or free-moving was separated into bins of equal length, typically 8 seconds each. Each bin of data was normalized to dF/F_0, where F_0 represented the 20th percentile of the data within that bin. In the meanwhile, we calculated the Pearson's correlation coefficient between the sequence of dF/F_0 values and the raw F sequence. If this correlation coefficient lower than 0.8, the mouse was excluded from the further analysis. The sum dFF activity was then determined by summing the resultant dF/F_0 values across all bins.

Statistical analysis

Sample sizes are represented in all figures as the number of mice included in the analysis. Statistical analysis was conducted using Prism V9.0 software (GraphPad Software, Inc.). For unpaired data, the non-parametric Mann-Whitney (M-W) test was employed, while one-way balanced ANOVA followed by Dunnet's multiple-comparison test was used for comparisons among multiple groups. Cumulative distributions were compared using the Kolmogorov-Smirnov (KS) test. The significance level was set at $P < 0.05$, denoted as $^*P < 0.05$, $^{**}P < 0.01$, and $^{***}P < 0.001$. Additionally, when the P-value fell between

0.05 and 0.1, it was labeled accordingly. Error bars in all figures represent the standard error of the mean (s.e.m).

References

1. Kalia LV, Lang AE. Parkinson's disease. The Lancet. 2015;386(9996):896-912.
2. Sveinbjornsdottir S. The clinical symptoms of Parkinson's disease. Journal of Neurochemistry. 2016;139(S1):318-24.
3. Dudman JT, Krakauer JW. The basal ganglia: from motor commands to the control of vigor. Current Opinion in Neurobiology. 2016;37:158-66.
4. Turner RS, Desmurget M. Basal ganglia contributions to motor control: a vigorous tutor. Current Opinion in Neurobiology. 2010;20(6):704-16.
5. Lemke SM, Ramanathan DS, Darevksy D, Egert D, Berke JD, Ganguly K. Coupling between motor cortex and striatum increases during sleep over long-term skill learning. Elife. 2021;10.
6. Santos FJ, Oliveira RF, Jin X, Costa RM. Corticostriatal dynamics encode the refinement of specific behavioral variability during skill learning. Elife. 2015;4:e09423.
7. Lemke SM, Ramanathan DS, Guo L, Won SJ, Ganguly K. Emergent modular neural control drives coordinated motor actions. Nat Neurosci. 2019;22(7):1122-31.
8. Gao LL, Wu T. The study of brain functional connectivity in Parkinson's disease. Transl Neurodegener. 2016;5:18.
9. Tessitore A, Cirillo M, De Micco R. Functional Connectivity Signatures of Parkinson's Disease. J Parkinsons Dis. 2019;9(4):637-52.
10. Filippi M, Sarasso E, Agosta F. Resting-state Functional MRI in Parkinsonian Syndromes. Mov Disord Clin Pract. 2019;6(2):104-17.
11. Lang S, Yoon EJ, Kibreab M, Kathol I, Cheetham J, Hammer T, et al. Mild behavioral impairment in Parkinson's disease is associated with altered corticostriatal connectivity. Neuroimage Clin. 2020;26:102252.
12. Mi TM, Zhang W, Li Y, Liu AP, Ren ZL, Chan P. Altered Functional Segregated Sensorimotor, Associative, and Limbic Cortical-Striatal Connections in Parkinson's Disease: An fMRI Investigation. Front Neurol. 2021;12:720293.
13. Rothkirch I, Granert O, Knutzen A, Wolff S, Gövert F, Pedersen A, et al. Dynamic causal modeling revealed dysfunctional effective connectivity in both, the cortico-basal-ganglia and the cerebello-cortical motor network in writers' cramp. Neuroimage Clin. 2018;18:149-59.
14. Unschuld PG, Joel SE, Liu X, Shanahan M, Margolis RL, Biglan KM, et al. Impaired cortico-striatal functional connectivity in prodromal Huntington's Disease. Neurosci Lett. 2012;514(2):204-9.
15. DeLong MR. Primate models of movement disorders of basal ganglia origin. Trends Neurosci. 1990;13(7):281-5.
16. McGregor MM, Nelson AB. Circuit Mechanisms of Parkinson's Disease. Neuron. 2019;101(6):1042-56.

17. Kravitz AV, Tye LD, Kreitzer AC. Distinct roles for direct and indirect pathway striatal neurons in reinforcement. Nat Neurosci. 2012;15(6):816-8.
18. Surmeier DJ, Ding J, Day M, Wang Z, Shen W. D1 and D2 dopamine-receptor modulation of striatal glutamatergic signaling in striatal medium spiny neurons. Trends Neurosci. 2007;30(5):228-35.
19. Tecuapetla F, Jin X, Lima SQ, Costa RM. Complementary Contributions of Striatal Projection Pathways to Action Initiation and Execution. Cell. 2016;166(3):703-15.
20. Jin X, Tecuapetla F, Costa RM. Basal ganglia subcircuits distinctively encode the parsing and concatenation of action sequences. Nat Neurosci. 2014;17(3):423-30.
21. Lee K, Masmanidis SC. Aberrant features of in vivo striatal dynamics in Parkinson's disease. J Neurosci Res. 2019;97(12):1678-88.
22. Sharott A, Vinciati F, Nakamura KC, Magill PJ. A Population of Indirect Pathway Striatal Projection Neurons Is Selectively Entrained to Parkinsonian Beta Oscillations. J Neurosci. 2017;37(41):9977-98.
23. Ketzef M, Spigolon G, Johansson Y, Bonito-Oliva A, Fisone G, Silberberg G. Dopamine Depletion Impairs Bilateral Sensory Processing in the Striatum in a Pathway-Dependent Manner. Neuron. 2017;94(4):855-65 e5.
24. Mallet N, Ballion B, Le Moine C, Gonon F. Cortical inputs and GABA interneurons imbalance projection neurons in the striatum of parkinsonian rats. J Neurosci. 2006;26(14):3875-84.
25. Parker PR, Lalive AL, Kreitzer AC. Pathway-Specific Remodeling of Thalamostriatal Synapses in Parkinsonian Mice. Neuron. 2016;89(4):734-40.
26. Parker JG, Marshall JD, Ahanonu B, Wu YW, Kim TH, Grewe BF, et al. Diametric neural ensemble dynamics in parkinsonian and dyskinetic states. Nature. 2018;557(7704):177-82.
27. Ryan MB, Bair-Marshall C, Nelson AB. Aberrant Striatal Activity in Parkinsonism and Levodopa-Induced Dyskinesia. Cell Rep. 2018;23(12):3438-46.e5.
28. Bloem BR, Okun MS, Klein C. Parkinson's disease. Lancet. 2021;397(10291):2284-303.
29. Luk KC, Kehm V, Carroll J, Zhang B, O'Brien P, Trojanowski JQ, et al. Pathological α-synuclein transmission initiates Parkinson-like neurodegeneration in nontransgenic mice. Science. 2012;338(6109):949-53.
30. Paumier KL, Luk KC, Manfredsson FP, Kanaan NM, Lipton JW, Collier TJ, et al. Intrastriatal injection of pre-formed mouse α-synuclein fibrils into rats triggers α-synuclein pathology and bilateral nigrostriatal degeneration. Neurobiol Dis. 2015;82:185-99.
31. Long H, Zheng W, Liu Y, Sun Y, Zhao K, Liu Z, et al. Wild-type α-synuclein inherits the structure and exacerbated neuropathology of E46K mutant fibril strain by cross-seeding. Proceedings of the National Academy of Sciences. 2021;118(20).
32. Brismar T. The human EEG--physiological and clinical studies. Physiol Behav. 2007;92(1-2):141-7.
33. Thompson JA, Lanctin D, Ince NF, Abosch A. Clinical implications of local field potentials for understanding and treating movement disorders. Stereotact Funct Neurosurg. 2014;92(4):251-63.
34. Lee MH, Smyser CD, Shimony JS. Resting-state fMRI: a review of methods and clinical applications. AJNR Am J Neuroradiol. 2013;34(10):1866-72.
35. Zhou ZC, Gordon-Fennell A, Piantadosi SC, Ji N, Smith SL, Bruchas MR, et al. Deep-brain optical recording of neural dynamics during behavior. Neuron. 2023;111(23):3716-38.
36. Tecuapetla F, Matias S, Dugue GP, Mainen ZF, Costa RM. Balanced activity in basal ganglia projection pathways is critical for contraversive movements. Nat Commun. 2014;5:4315.

37. Cui G, Jun SB, Jin X, Pham MD, Vogel SS, Lovinger DM, et al. Concurrent activation of striatal direct and indirect pathways during action initiation. Nature. 2013;494(7436):238-42.
38. Shin JH, Kim D, Jung MW. Differential coding of reward and movement information in the dorsomedial striatal direct and indirect pathways. Nat Commun. 2018;9(1):404.
39. Bell PT, Gilat M, O'Callaghan C, Copland DA, Frank MJ, Lewis SJ, et al. Dopaminergic basis for impairments in functional connectivity across subdivisions of the striatum in Parkinson's disease. Hum Brain Mapp. 2015;36(4):1278-91.
40. Hensel L, Hoffstaedter F, Caspers J, Michely J, Mathys C, Heller J, et al. Functional Connectivity Changes of Key Regions for Motor Initiation in Parkinson's Disease. Cereb Cortex. 2019;29(1):383-96.
41. Long H, Zheng W, Liu Y, Sun Y, Zhao K, Liu Z, et al. Wild-type α-synuclein inherits the structure and exacerbated neuropathology of E46K mutant fibril strain by cross-seeding. Proc Natl Acad Sci U S A. 2021;118(20).
42. Crompe B, Aristieta A, Leblois A, Elsherbiny S, Boraud T, Mallet NP. The globus pallidus orchestrates abnormal network dynamics in a model of Parkinsonism. Nat Commun. 2020;11(1):1570.
43. Perlbarg V, Lambert J, Butler B, Felfli M, Valabrègue R, Privat AL, et al. Alterations of the nigrostriatal pathway in a 6-OHDA rat model of Parkinson's disease evaluated with multimodal MRI. PLoS One. 2018;13(9):e0202597.
44. Beck MH, Haumesser JK, Kuhn J, Altschuler J, Kuhn AA, van Riesen C. Short- and long-term dopamine depletion causes enhanced beta oscillations in the cortico-basal ganglia loop of parkinsonian rats. Exp Neurol. 2016;286:124-36.
45. Evangelisti S, Pittau F, Testa C, Rizzo G, Gramegna LL, Ferri L, et al. L-Dopa Modulation of Brain Connectivity in Parkinson's Disease Patients: A Pilot EEG-fMRI Study. Front Neurosci. 2019;13:611.
46. Costa VD, Tran VL, Turchi J, Averbeck BB. Dopamine modulates novelty seeking behavior during decision making. Behav Neurosci. 2014;128(5):556-66.
47. Kesner AJ, Calva CB, Ikemoto S. Seeking motivation and reward: Roles of dopamine, hippocampus, and supramammillo-septal pathway. Prog Neurobiol. 2022;212:102252.
48. Chinta SJ, Andersen JK. Dopaminergic neurons. Int J Biochem Cell Biol. 2005;37(5):942-6.
49. Wu T, Liu J, Zhang H, Hallett M, Zheng Z, Chan P. Attention to Automatic Movements in Parkinson's Disease: Modified Automatic Mode in the Striatum. Cereb Cortex. 2015;25(10):3330-42.
50. Wu T, Wang L, Hallett M, Chen Y, Li K, Chan P. Effective connectivity of brain networks during self-initiated movement in Parkinson's disease. Neuroimage. 2011;55(1):204-15.
51. Luo C, Song W, Chen Q, Zheng Z, Chen K, Cao B, et al. Reduced functional connectivity in early-stage drug-naive Parkinson's disease: a resting-state fMRI study. Neurobiol Aging. 2014;35(2):431-41.
52. Le W, Dong J, Li S, Korczyn AD. Can Biomarkers Help the Early Diagnosis of Parkinson's Disease? Neurosci Bull. 2017;33(5):535-42.
53. Ellmore TM, Castriotta RJ, Hendley KL, Aalbers BM, Furr-Stimming E, Hood AJ, et al. Altered nigrostriatal and nigrocortical functional connectivity in rapid eye movement sleep behavior disorder. Sleep. 2013;36(12):1885-92.
54. Ereira S, Waters S, Razi A, Marshall CR. Early detection of dementia with default-mode network effective connectivity. Nature Mental Health. 2024.

55. Rossini PM, Miraglia F, Alu F, Cotelli M, Ferreri F, Iorio RD, et al. Neurophysiological Hallmarks of Neurodegenerative Cognitive Decline: The Study of Brain Connectivity as A Biomarker of Early Dementia. J Pers Med. 2020;10(2).
56. Varela F, Lachaux JP, Rodriguez E, Martinerie J. The brainweb: phase synchronization and large-scale integration. Nat Rev Neurosci. 2001;2(4):229-39.
57. Harris AZ, Gordon JA. Long-range neural synchrony in behavior. Annu Rev Neurosci. 2015;38:171-94.
58. Gatev P, Darbin O, Wichmann T. Oscillations in the basal ganglia under normal conditions and in movement disorders. Mov Disord. 2006;21(10):1566-77.
59. Ashby FG, Turner BO, Horvitz JC. Cortical and basal ganglia contributions to habit learning and automaticity. Trends in Cognitive Sciences. 2010;14(5):208-15.
60. Wurster CD, Graf H, Ackermann H, Groth K, Kassubek J, Riecker A. Neural correlates of rate-dependent finger-tapping in Parkinson's disease. Brain Struct Funct. 2015;220(3):1637-48.
61. Bologna M, Leodori G, Stirpe P, Paparella G, Colella D, Belvisi D, et al. Bradykinesia in early and advanced Parkinson's disease. J Neurol Sci. 2016;369:286-91.
62. Tessitore A, Giordano A, De Micco R, Russo A, Tedeschi G. Sensorimotor connectivity in Parkinson's disease: the role of functional neuroimaging. Front Neurol. 2014;5:180.
63. Chen Z, Zhang ZY, Zhang W, Xie T, Li Y, Xu XH, et al. Direct and indirect pathway neurons in ventrolateral striatum differentially regulate licking movement and nigral responses. Cell Rep. 2021;37(3):109847.
64. Sheng MJ, Lu D, Shen ZM, Poo MM. Emergence of stable striatal D1R and D2R neuronal ensembles with distinct firing sequence during motor learning. Proc Natl Acad Sci U S A. 2019;116(22):11038-47.
65. Burke DA, Rotstein HG, Alvarez VA. Striatal Local Circuitry: A New Framework for Lateral Inhibition. Neuron. 2017;96(2):267-84.
66. Obeso JA, Marin C, Rodriguez-Oroz C, Blesa J, Benitez-Temiño B, Mena-Segovia J, et al. The basal ganglia in Parkinson's disease: current concepts and unexplained observations. Ann Neurol. 2008;64 Suppl 2:S30-46.
67. Escande MV, Taravini IR, Zold CL, Belforte JE, Murer MG. Loss of Homeostasis in the Direct Pathway in a Mouse Model of Asymptomatic Parkinson's Disease. J Neurosci. 2016;36(21):5686-98.
68. Chen Y, Hong Z, Wang J, Liu K, Liu J, Lin J, et al. Circuit-specific gene therapy reverses core symptoms in a primate Parkinson's disease model. Cell. 2023;186(24):5394-410 e18.
69. Obeso JA, Rodriguez-Oroz M, Marin C, Alonso F, Zamarbide I, Lanciego JL, et al. The origin of motor fluctuations in Parkinson's disease: importance of dopaminergic innervation and basal ganglia circuits. Neurology. 2004;62(1 Suppl 1):S17-30.
70. Zhai S, Tanimura A, Graves SM, Shen W, Surmeier DJ. Striatal synapses, circuits, and Parkinson's disease. Curr Opin Neurobiol. 2018;48:9-16.
71. Cramb KML, Beccano-Kelly D, Cragg SJ, Wade-Martins R. Impaired dopamine release in Parkinson's disease. Brain. 2023;146(8):3117-32.
72. Costa RM, Lin SC, Sotnikova TD, Cyr M, Gainetdinov RR, Caron MG, et al. Rapid alterations in corticostriatal ensemble coordination during acute dopamine-dependent motor dysfunction. Neuron. 2006;52(2):359-69.

73. Herz DM, Haagensen BN, Christensen MS, Madsen KH, Rowe JB, Løkkegaard A, et al. Abnormal dopaminergic modulation of striato-cortical networks underlies levodopa-induced dyskinesias in humans. Brain. 2015;138(Pt 6):1658-66.
74. Tozzi A, Sciaccaluga M, Loffredo V, Megaro A, Ledonne A, Cardinale A, et al. Dopamine-dependent early synaptic and motor dysfunctions induced by alpha-synuclein in the nigrostriatal circuit. Brain. 2021;144(11):3477-91.
75. Burke RE, O'Malley K. Axon degeneration in Parkinson's disease. Exp Neurol. 2013;246:72-83.
76. Zong FJ, Min X, Zhang Y, Li YK, Zhang XT, Liu Y, et al. Circadian time- and sleep-dependent modulation of cortical parvalbumin-positive inhibitory neurons. EMBO J. 2023;42(3):e111304.
77. Kato HK, Asinof SK, Isaacson JS. Network-Level Control of Frequency Tuning in Auditory Cortex. Neuron. 2017;95(2):412-23 e4.
78. Hu H, Gan J, Jonas P. Interneurons. Fast-spiking, parvalbumin(+) GABAergic interneurons: from cellular design to microcircuit function. Science. 2014;345(6196):1255263.
79. Mallet N, Le Moine C, Charpier S, Gonon F. Feedforward inhibition of projection neurons by fast-spiking GABA interneurons in the rat striatum in vivo. J Neurosci. 2005;25(15):3857-69.
80. Gittis AH, Kreitzer AC. Striatal microcircuitry and movement disorders. Trends Neurosci. 2012;35(9):557-64.
81. Chen H, Lei H, Xu Q. Neuronal activity pattern defects in the striatum in awake mouse model of Parkinson's disease. Behav Brain Res. 2018;341:135-45.

Figures and Legends

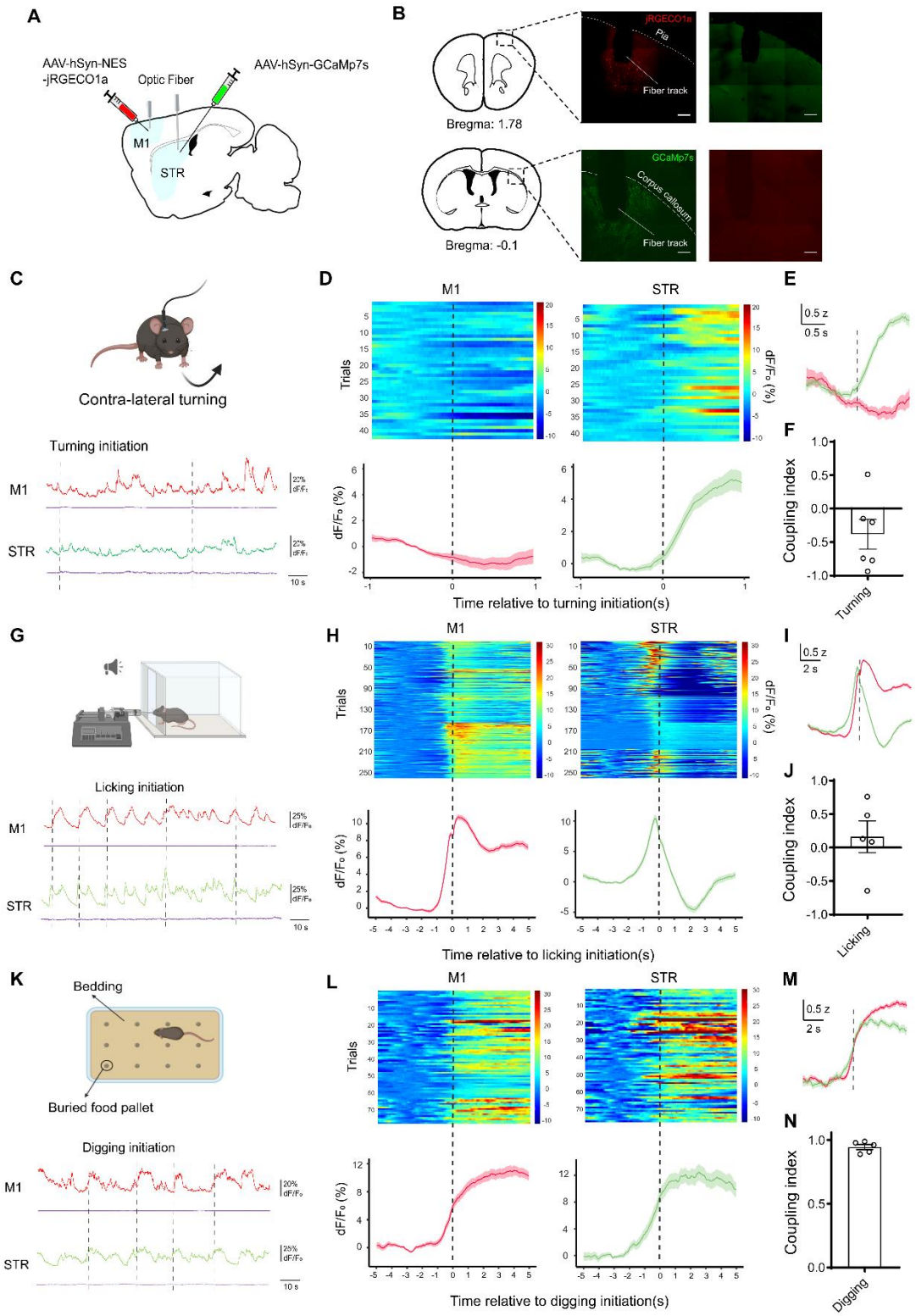

Figure 1. Detection of task-specific cortico-striatal coupling via dual fiber photometry imaging

A. Scheme of virus injection and optic fiber implantation.

B. Anatomical verification of virus expression and optic fiber localization. Scale bar: 200μm.

C-N. Examination of the cortico-striatal couplings during contralateral turning (C-F), licking (G-J), and digging (K-N).

(C, G, K) Behavioral diagrams (top) and example Ca^{2+} activities recorded from the primary motor cortex (M1, red) and the striatum (STR, green) with dotted lines denoted onsets of the specified behaviors. Ca^{2+}-independent fluorescence was monitored using 405 nm light pulses for individual channel (purple, bottom).

(D, H, L) Heatmaps showing all compiled trials (Top panels) and the averaged Ca^{2+} signal intensities (dF/F_0, bottom panels) aligned (dotted lines) to the initiation of the contralateral turning (D), licking (H), and digging (L). All left panels, M1 signal; all right panels, STR signals.

(E, I, M) Temporally aligned traces showing z-scored average signal intensities of both M1 (red) and STR (green).

(F, J, N) Calculated cortico-striatal coupling indices for contralateral turning (F), licking (J), and digging (N).

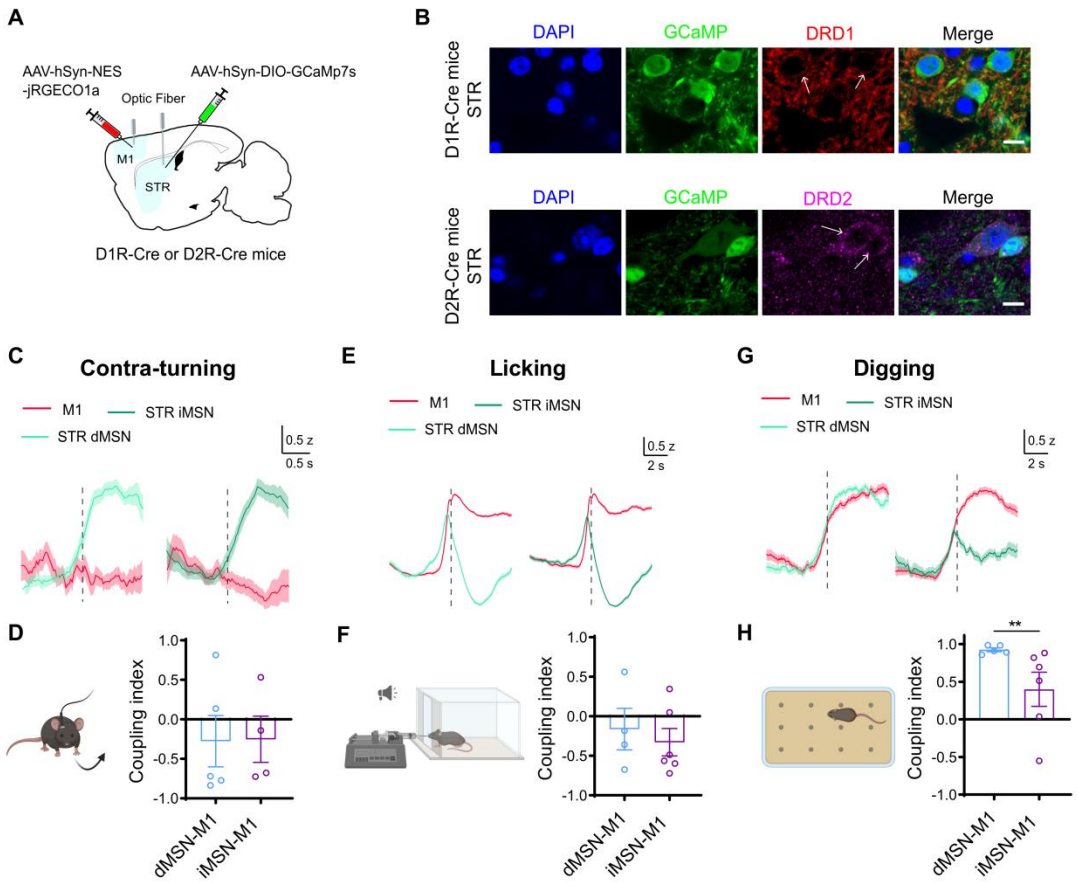

Figure 2. Task- and cell type-specific cortico-striatal coupling

A. Schematic diagram showing the experimental design for analyzing cell type-specific cortico-striatal coupling.

B. Immunofluorescence images showing the colocalization between DRD1 (red) and DIO-GCaMP (green) in D1R-Cre mice (top panels), and the colocalization between DRD2 (magenta) and DIO-GCaMP (green) in the D2R-Cre mice (bottom panels). Scale bar: 10μm.

C, E, G. Z-scored average traces of M1 (red) and STR dMSN (light green) and iMSN (dark green) Ca^{2+} activities temporally aligned to the initiation of contralateral turning (C), licking (E), and digging (G).

D, F, H. Comparison of cell type-specific cortico-striatal coupling indices for turning (D), licking (F), and digging behavior (H, P = 0.0087). Mann-Whitney test. **P<0.01.

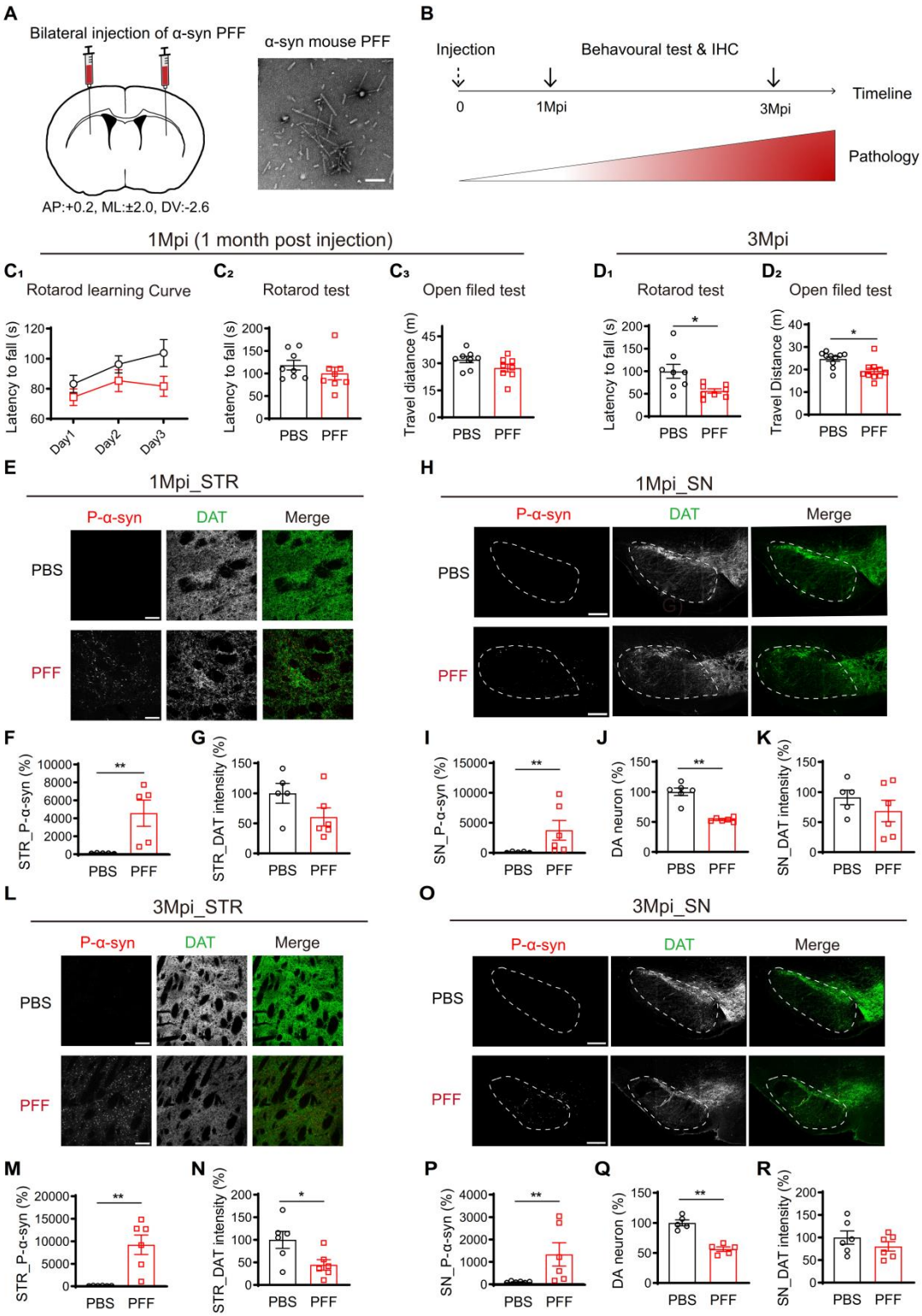

Figure 3. Pathological characterization of α-synuclein preformed fibril (PFF) induced PD-like mouse model

A. Schematic diagram describing the bilateral inoculation of PFF into striatum of wildtype mice. Right panel, transmitted electron microscope image of PFF. Scale bar: 100 nm.

B. Experimental timeline. IHC: Immunohistochemistry.

C-D. Behavioral analysis of the PFF- and PBS-injected mice 1 (C) and 3 (D) months post injection (Mpi).

(C_1) Learning curve of rotarod running.

(C_2) Latency to fall in the rotarod test.

(C_3) Total travel distance in the open field test.

(D_1) Latency to fall in the rotarod test 3Mpi (P = 0.0207).

(D_2) Total travel distance in the open field test 3Mpi (*P* = 0.0147).

E-K. Immunofluorescence analyses of pathological hallmarks in PFF- and PBS-injected mice 1Mpi. All data normalized to PBS control.

(E-G) Comparison of the p-α-Syn intensity (F, *P* = 0.0079) and dopamine transporter (DAT) signal intensities (G) in STR. E, Representative immunofluorescence images. Scale bars: 50 μm.

(H-K) Comparison of the p-α-Syn intensity (I, *P* = 0.0043), DA neuron number (J, *P* = 0.0022) and DAT intensity (K) in substantia nigra (SN). H, Representative immunofluorescence images. Scale bars: 250 μm.

L-R. Immunofluorescence analyses of pathological hallmarks in PFF- and PBS-injected mice 3Mpi. All data normalized to PBS control.

(L-N) Comparison of the p-α-Syn intensity (M, *P* = 0.0022) and dopamine transporter (DAT) signal intensities (N, *P* =0.0411) in STR. L, Representative immunofluorescence images. Scale bars: 100 μm.

(O-R) Comparison of the p-α-Syn intensity (P, *P* =0.0022), DA neuron number (Q, *P* = 0.0079) and DAT intensity (R) in SN. O, Representative immunofluorescence images. Scale bars: 250 μm.

Mann-Whitney test, unless otherwise noted. Two-way ANOVA with Sidak's multiple comparisons test (C_1). *P<0.05, **P<0.01.

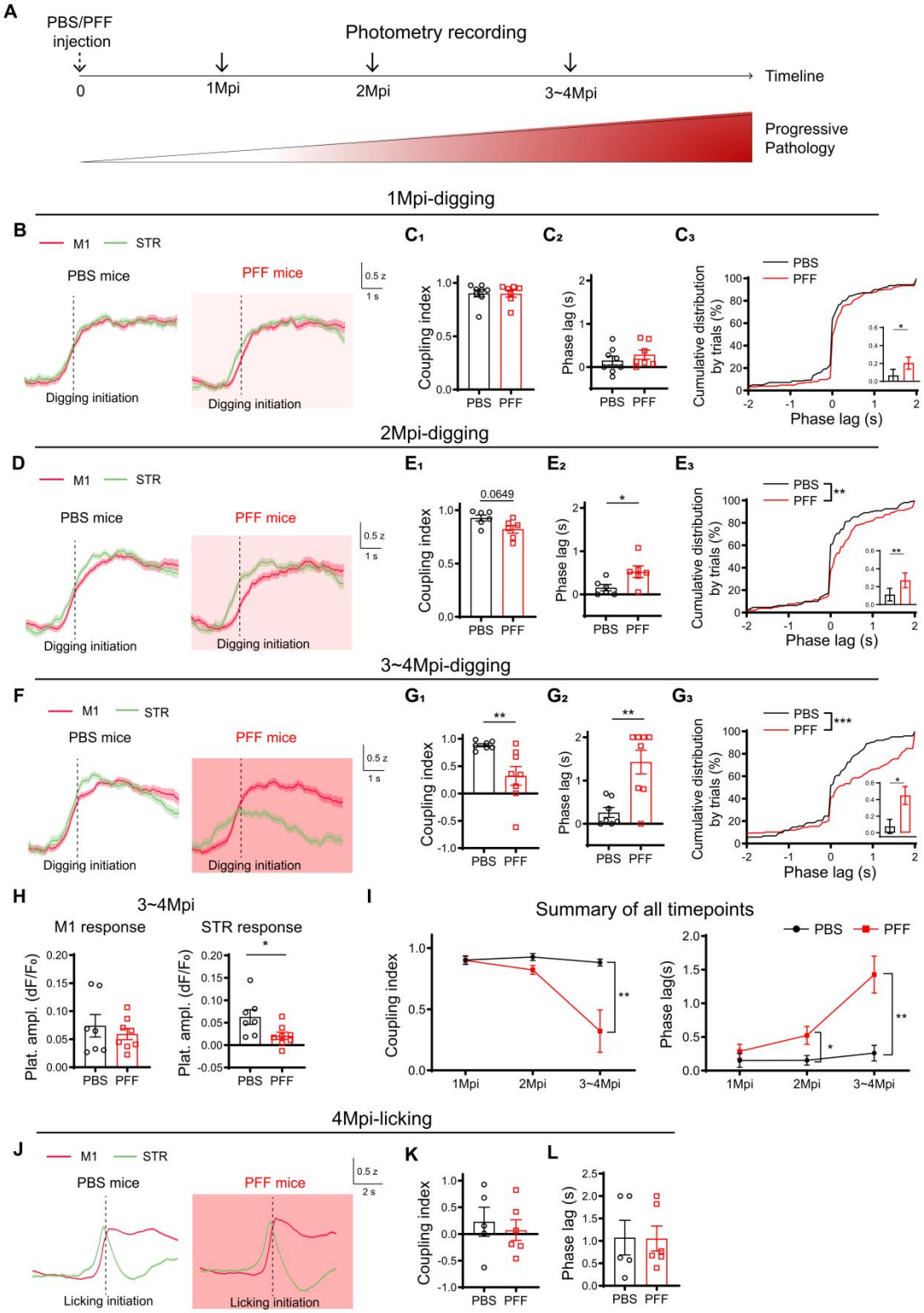

Figure 4. Task-specific cortico-striatal decoupling in PD-like mice

A. Experimental timeline.

B-I, Dual fiber photometry imaging of M1 and STR in PFF- and PBS-injected mice at 1 Mpi (B-C), 2 Mpi (D-E), and 3-4 Mpi (F-I) during digging.

(B, D, F) Z-scored average traces of M1 (red) and STR (green) Ca^{2+} activities temporally aligned to the initiation of digging. Left, PBS; Right, PFF.

(C, E, G) Quantitative analyses of the cortico-striatal coupling.

(C_1, E_1, G_1) Coupling indices (E_1, P = 0.0649. G_1, P = 0.0037).

(C_2, E_2, G_2) Phase lags (E_2, P = 0.0281. G_2, P = 0.0082).

(C_3, E_3, G_3) Cumulative distribution of phase lag per trial (C_3: PBS = 140 trials, PFF = 124 trials. E_3: PBS = 109 trials, PFF = 104 trials; P = 0.0041. G_3: PBS = 102 trials, PFF = 118 trials; P = 0.0009. Kolmogorov-Smirnov test). Inserts, Comparison of the trial average phase lag (In C_3, P = 0.0188. In E_3, P = 0.0072. In G_3, P = 0.0110).

(H) Plateau amplitude of M1 (left) and STR (right) Ca^{2+} activities at 3~4Mpi.

(I) The temporal profiles of coupling index (left) and phase lag (right).

J-K. Dual fiber photometry imaging of M1 and STR at 4 Mpi during licking.

(J) Z-scored average traces of M1 (red) and STR (green) Ca^{2+} activities temporally aligned to the initiation of licking.

(K) Comparison of the coupling indices.

(L) Comparison of the phase lags.

Mann-Whitney test, unless otherwise noted. *P<0.05. **P<0.01. ***P<0.001.

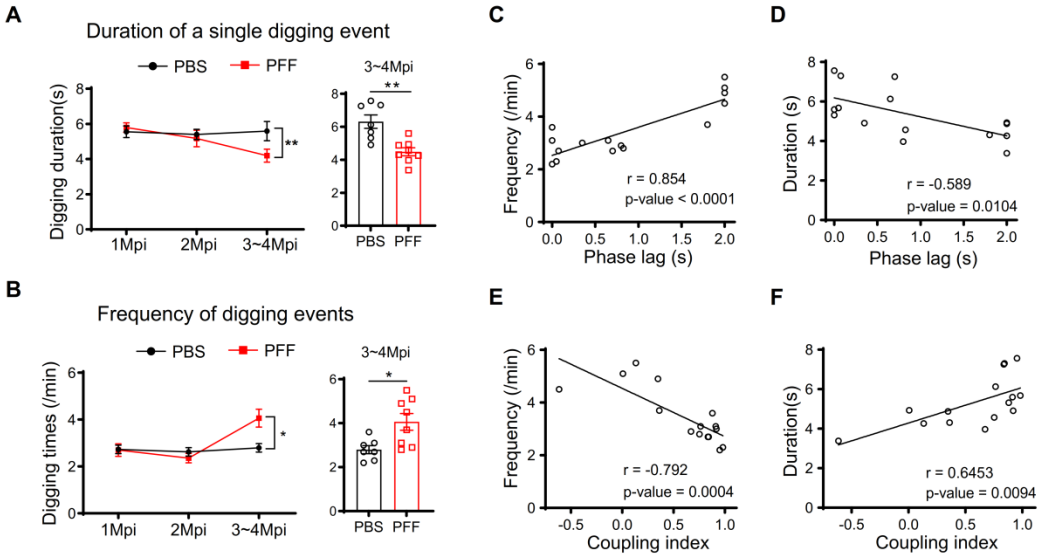

Figure 5. Digging-associated cortico-striatal decoupling correlated with specific behavioral deficits

A. Duration of a single digging event. Left, the temporal profiles of average digging duration. Right, comparison of the duration at 3~4Mpi (P = 0.0022).

B. Frequency of digging events. Left, temporal profiles of digging frequency. Right, comparison of the frequency at 3~4Mpi (P = 0.0152).

C, D. Correlation analysis of phase lag between digging frequency (C) and duration (D) from PBS- and PFF-injected mice at 3~4Mpi. r: Pearson's correlation coefficient. Each dot represents data from an individual mouse (the same below).

E, F. Correlation analysis of coupling index between digging frequency (E) and duration (F) from PBS- and PFF-injected mice at 3~4Mpi.

Mann-Whitney test. *P<0.05. **P<0.01.

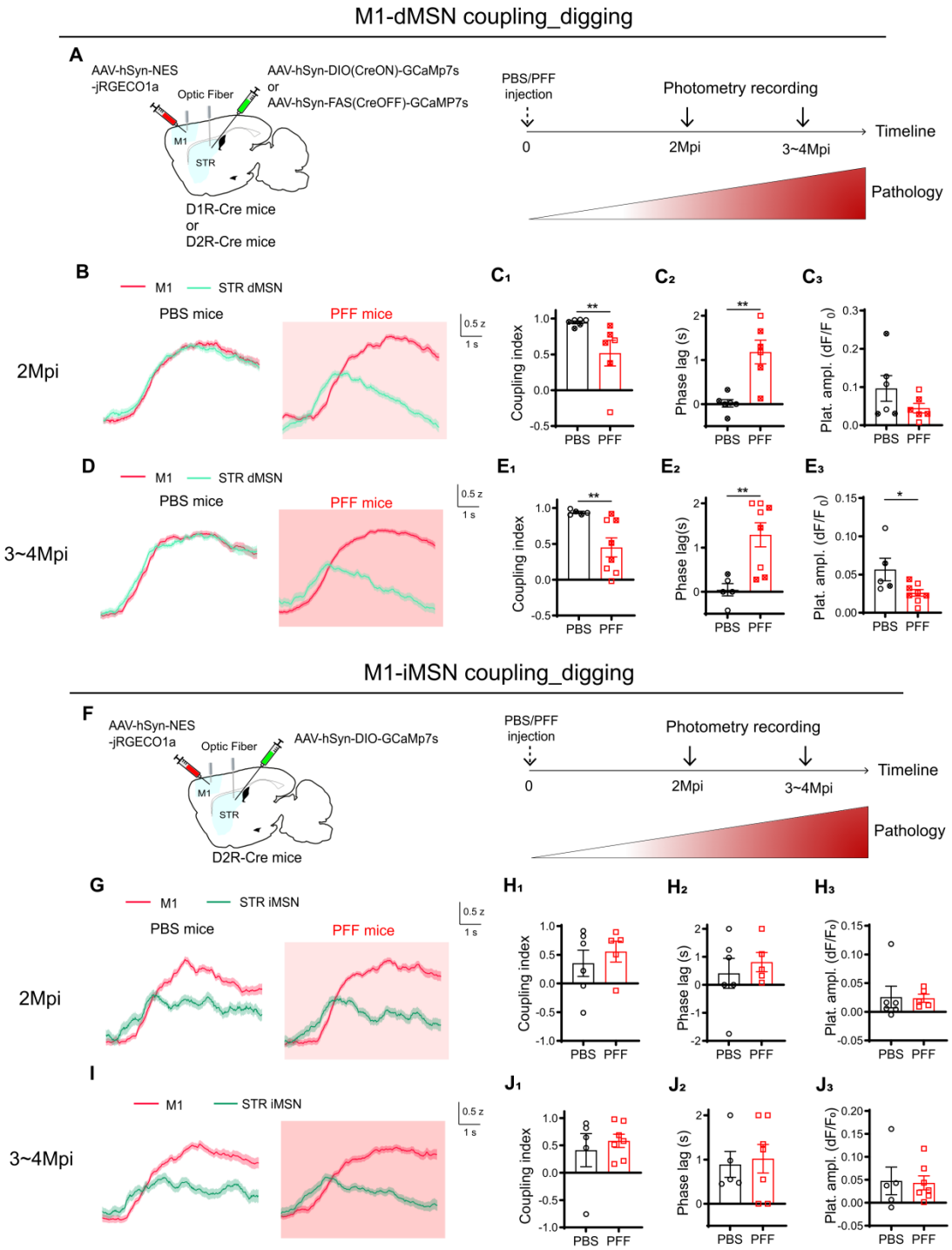

Figure 6. Cell type-specific contribution of digging-related cortico-striatal decoupling in PFF-injected mice

A-E. Dual fiber photometry imaging of M1 and striatal dMSN in PFF- and PBS-injected mice at 2 Mpi (B-C), and 3-4 Mpi (D-E) during digging.

(A) Scheme of virus injection and optic fiber implantation. Note the CreON-GCaMP virus was injected into the STR of D1R-Cre mice, while CreOFF-GCaMP virus was injected into the STR of D2R-Cre mice.

884 Right panel, experiment timeline.

885 (B, D) Z-scored average traces of M1 (red) and STR dMSN (aqua) Ca^{2+} activities temporally aligned to

886 the initiation of digging. Left, PBS; Right, PFF.

887 (C, E) Quantitative analyses of the M1-dMSN coupling and plateau amplitude of dMSN Ca^{2+} activities

888 at 2 Mpi (C) and 3-4 Mpi (E). The hollow signal represents D1R-Cre mice; the cross signal represents

889 D2-Cre mice.

890 (C_1, E_1) Coupling indices (C_1, P = 0.0043. E_1, P = 0.0062).

891 (C_2, E_2) Phase lags (E_2, P = 0.0043. G_2, P = 0.0062).

892 (C_3, E_3) Plateau amplitude of dMSN Ca^{2+} activities (E_3, P = 0.0451).

893 **F-J.** Dual fiber photometry imaging of M1 and striatal iMSN in PFF- and PBS-injected mice at 2 Mpi (G-

894 H), and 3-4 Mpi (I-J) during digging. Right panel, experiment timeline.

895 (F) Scheme of virus injection and optic fiber implantation.

896 (G, I) Z-scored average traces of M1 (red) and striatal iMSN (dark green) Ca^{2+} activities temporally

897 aligned to the initiation of digging. Left, PBS; Right, PFF.

898 (H, J) Quantitative analyses of the M1-iMSN coupling and plateau amplitude of iMSN Ca^{2+} activities at

899 2 Mpi (H) and 3-4 Mpi (J).

900 (H_1, J_1) Comparison of the coupling indices.

901 (H_2, J_2) Comparison of the phase lags.

902 (H_3, J_3) Comparison of the plateau amplitude of iMSN Ca^{2+} activities.

903 Mann-Whitney test. *P<0.05. **P<0.01.

904

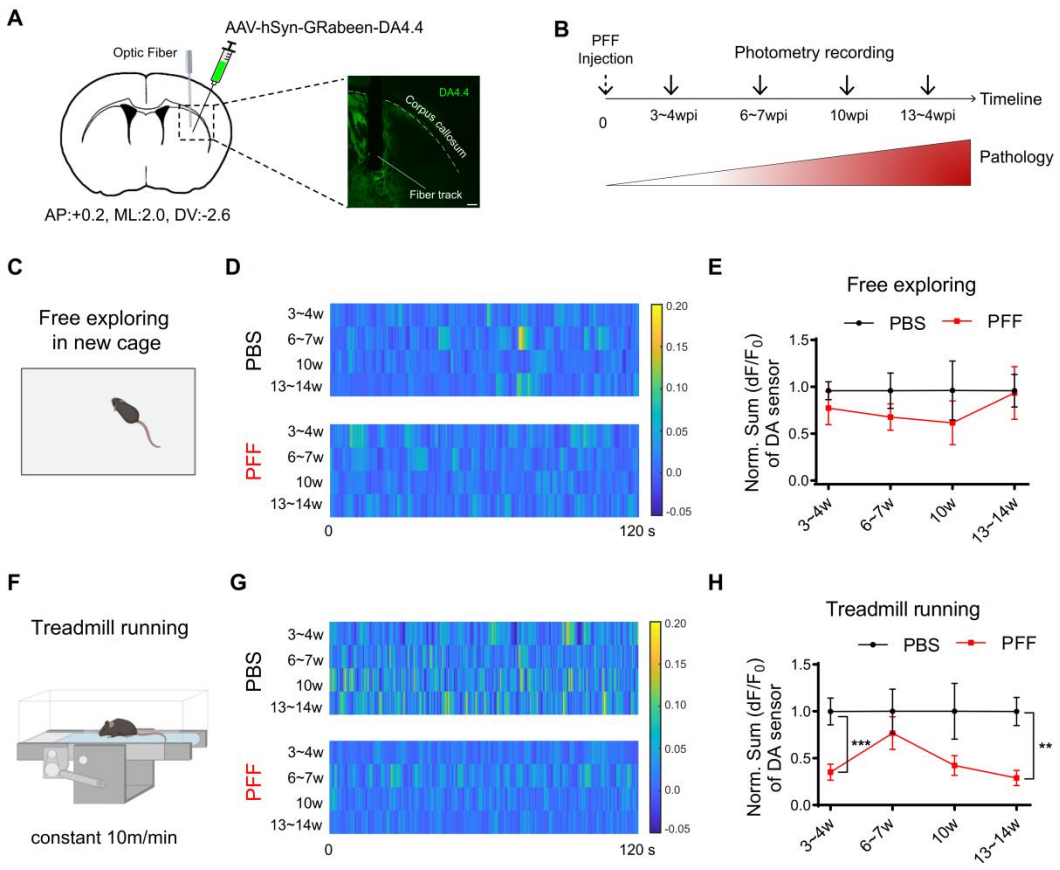

Figure 7 Cortico-striatal decoupling in PFF-injected mice accompanied by deficiency of striatal extracellular dopamine

A. Schematic diagram showing the experimental design for assessing striatal extracellular dopamine (DA) level. DA4.4 is a florescence-based DA sensor. Right panel, anatomical verification of virus expression and optic fiber localization. Scale bar: 200μm.

B. Experimental timeline.

C. Schematic diagram for free-exploring paradigm.

D. Representative magnitude heatmap of normalized (dF/F_0) of DA sensor activity 3~4 weeks post-injection (wpi), 6~7wpi, 10wpi, and 13~14wpi from one PBS-injected mouse and one PFF-injected mouse during 2-minute free-exploring.

E. Normalized sum activity of DA sensor during free-exploring from PBS- and PFF-injected mice 3~4wpi, 6~7wpi, 10wpi, 13~14wpi. Data batch-normalized to the PBS group (the same below).

F.Schematic diagram for treadmill running paradigm.

G. Representative magnitude heatmap of normalized (dF/F_0) of DA sensor activity 3~4wpi, 6~7wpi, 10wpi, and 13~14wpi from same two mice as in (D) during 2-minute treadmill running.

921 **H**. Normalized sum activity of DA sensor during free-exploring from PBS- and PFF-injected mice at

922 3~4wpi (P = 0.0007), 6~7wpi, 10wpi, 13~14wpi (P = 0.0043).

923 Mann-Whitney test. **P<0.01. ***P<0.001.

924

925

926

927

928

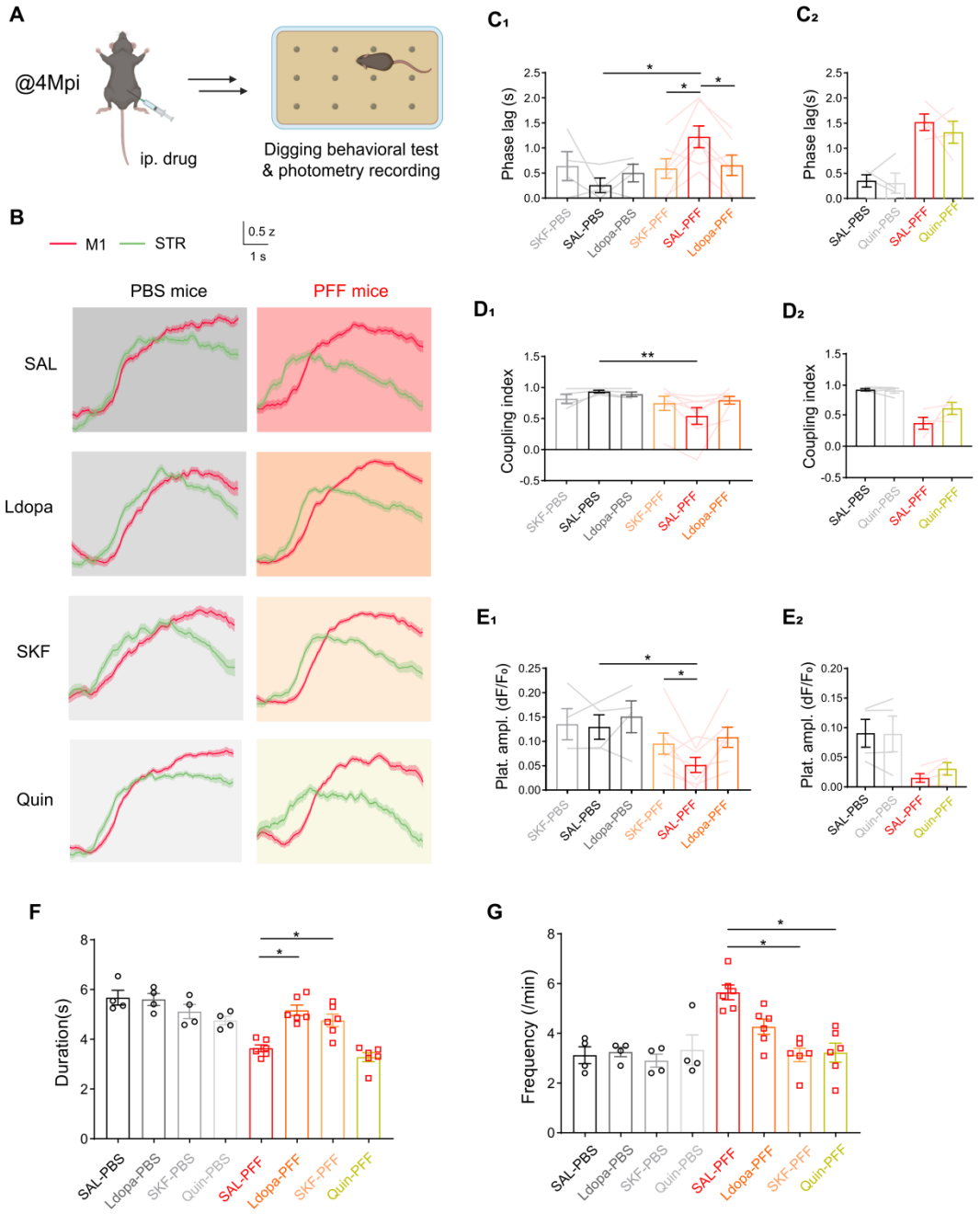

Figure 8 Selective activation to D1R rescues both digging-associated cortico-striatal decoupling and digging behavioral defects

A. Schematic diagram for pharmacological experiments. i.p., intraperitoneal administration.

B-E. Dual fiber photometry imaging of M1 and STR in PFF- and PBS-injected mice at 4Mpi during digging, after ip. SAL (saline), L-dopa, SKF (SKF-81297, a D1R selective agonist), or Quin (quinpirole, a D2R selective agonist).

(B) Z-scored average traces of M1 (red) and STR (green) temporally aligned, digging-associated Ca^{2+} activities after administration of drugs. Left, PBS; Right, PFF.

(C, D, E) Quantitative analyses of the digging-associated cortico-striatal coupling (C,D) and amplitude of striatal Ca^{2+} activities (E) after administration of drugs.

(C_1) Comparison of the phase lags (SAL-PBS *vs.* SAL-PFF: Mann-Whitney test, P = 0.0152. PFF groups: SAL-PFF as control, $F_{(1.588, 9.529)}$ = 9.270, SAL-PFF *vs.* Ldopa-PFF, P =0.0156; SAL-PFF vs. SKF-PFF, P = 0.0328).

(C_2) Comparison of the phase lags, after saline or quinpirole administration.

(D_1) Comparison of the coupling indices (SAL-PBS *vs.* SAL-PFF: Mann-Whitney test, P = 0.0043).

(D_2) Comparison of the coupling indices, after saline or quinpirole administration.

(E_1) Comparison of the plateau amplitude of striatal activity (SAL-PBS *vs.* SAL-PFF: Mann-Whitney test, P = 0.0424. PFF groups: SAL-PFF as control, $F_{(1.453, 8.719)}$ = 6.152, SAL-PFF vs. SKF-PFF, P = 0.0459).

(E_2) Comparison of the plateau amplitude of striatal activity, after saline or quinpirole administration.

F-G. Effect of dopaminergic drugs on digging behavior.

(F) Comparison of digging duration (PFF groups: SAL-PFF as control, $F_{(1.463, 7.317)}$ = 19.97, SAL-PFF *vs.* Ldopa-PFF, P = 0.0018; SAL-PFF *vs.* SKF-PFF, P = 0.0388).

(G) Comparison of digging frequency (PFF groups: SAL-PFF as control, $F_{(2.120, 10.60)}$ = 11.78, SAL-PFF *vs.* SKF-PFF, P = 0.0143; SAL-PFF *vs.* Quin-PFF, P = 0.0192).

One-way ANOVA followed by Dunnett's multiple comparisons test, unless otherwise noted. Wilcoxon matched-pairs test (C_2, D_2, E_2). *P<0.05. **P<0.01.